Internal Diffraction of Ultrasound in Crystals: Phonon Focusing at Long Wavelengths

Matt R. Hauser,[1] R. L. Weaver,[2] and J. P. Wolfe[1]

[1]*Department of Physics and Materials Research Laboratory, University of Illinois at Urbana-Champaign, Urbana, Illinois 61801*
[2]*Department of Theoretical and Applied Mechanics, University of Illinois at Urbana-Champaign, Urbana, Illinois 61801*

(Received 24 February 1992)

We have obtained images of acoustic energy flux in anisotropic media by an ultrasonic analog to ballistic-phonon imaging. The observed flux reveals a phonon-focusing pattern modulated by interference fringes, in accord with prior theoretical predictions. While phonon imaging is largely restricted to insulators at low temperatures, the ultrasonic technique works at ambient temperatures and is also applicable to metals and even noncrystalline anisotropic materials.

PACS numbers: 62.30.+d, 43.35.+d, 62.65.+k, 63.20.−e

In elastically anisotropic materials, the direction of energy propagation for an elastic wave is in general not collinear with its wave vector. Because of this, vibrations emanating from a point source on one surface do not uniformly illuminate the opposite surface of the material. Instead, some regions receive very intense energy flux, while other regions receive very little. This anisotropic propagation of elastic energy, known as phonon focusing [1,2], has been studied extensively by phonon-imaging techniques using phonons in the 100-GHz range [3]. Such experiments have been particularly effective in characterizing the interactions of phonons with electrons, defects, and interfaces.

Figure 1(a) is an experimental image of the phonon-focusing pattern for silicon at 2 K [4]. This image displays the ballistic heat flux emanating from a point on the surface of the crystal excited by a focused laser beam; the bright lines represent caustics in the phonon flux, as predicted by elasticity theory. In this frequency range, phonons are ballistic only at low temperatures and in nonmetals because phonon-phonon and electron-phonon scattering limit their mean free paths, thereby destroying the focusing effect. The scattering depends strongly on frequency, however, and drops off rapidly towards lower frequencies, suggesting that the applicability of these imaging techniques can be greatly expanded by employing lower frequencies.

In addition to scattering less, low-frequency acoustic waves can be produced coherently and have macroscopic wavelengths (e.g., 300 μm for 15-MHz waves in Si). In contrast, the heat-pulse experiment of Fig. 1(a) involves incoherent phonons with wavelengths of a few hundred angstroms. The effect of finite wavelengths on a phonon-focusing pattern has been theoretically examined by Maris [5], although the predicted effects have not been observed with high-frequency heat pulses. The predictions call for the broadening of the sharp caustic structures and the occurrence of fringes, reminiscent of the diffraction of light around the edges of an obstacle. The physical cause of this internal diffraction, however, is quite different from optical diffraction because the caustics are caused not by solid obstructions, but by the elastic anisotropy of the crystal. In this Letter, we present the first observation of this internal diffraction effect by a

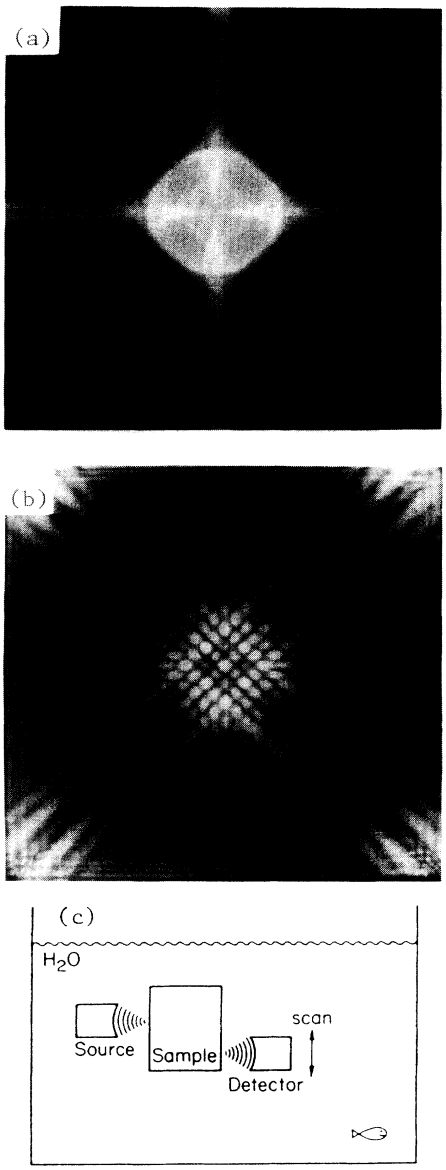

FIG. 1. (a) High-frequency phonon image of a (100)-oriented 2-cm silicon cube (1.5-cm × 1.5-cm scan range). (b) 15-MHz ultrasound image of the same 2-cm silicon cube over the entire face (500-ns pulse). (c) Schematic of ultrasound experiment.

technique akin to the phonon-imaging methods, but employing ultrasound instead of high-frequency phonons [6]. We show that phonon-focusing patterns can be obtained at room temperatures and through crystalline metals, as well as through noncrystalline anisotropic materials.

Recent work by Every and co-workers [7,8] has demonstrated the anisotropic propagation of ultrasound in silicon using an intense pulsed laser beam as a scannable thermoelastic source, and a 1-mm-aperture piezoelectric detector attached to the crystal. While this configuration yielded a method for precise measurement of elastic constants and observation of pseudosurface waves, it lacked sufficient spatial resolution for imaging experiments. Our present experiments utilize tone-burst pulses of 15 MHz ultrasound (typically about 500 ns long) which are produced and detected by two acoustic transducers which focus an ultrasound beam to a diameter of approximately 200 μm in water as illustrated in Fig. 1(c). One transducer is held fixed relative to the sample, and the other is scanned in two dimensions in the plane of the sample face. The received pulses are rectified and then time selected by a boxcar integrator.

Figure 1(b) is an ultrasound image of silicon obtained with a broad boxcar gate to admit signals from the pseudotransverse propagation modes over a wide scan range. The general concentration of acoustic flux is similar to the thermal flux in the phonon image of Fig. 1(a); however, the ultrasound image shows striking effects due to acoustic interference.

We now give a physical explanation of this internal diffraction of acoustic waves. In the far field, where the source-to-detector distance is much greater than the source size and the wavelength, the waves arriving at the detector may be viewed as plane waves with wave vector $\mathbf{k}$. Figure 2(a) shows a constant-frequency contour in k space for the slow-transverse (ST) mode in silicon. The dots are "parabolic points" of zero curvature. Vibrations with wave vector $\mathbf{k}_0$ propagate with a group velocity $\mathbf{v}_0=\nabla_k\omega(\mathbf{k}_0)$, normal to the constant-ω surface at $\mathbf{k}_0$, arriving at a point $\mathbf{R}_0$ on the opposite surface of the crystal. At zero-curvature points such as $\mathbf{k}_0$, neighboring $\mathbf{k}$'s have nearly the same group velocity as $\mathbf{k}_0$. This gives rise to the high-intensity caustics in the heat-pulse experiment. If, as shown in Fig. 2(b), the detector is moved to a point $\mathbf{R}_1$ slightly away from $\mathbf{R}_0$, two distinct waves with wave vectors $\mathbf{k}_1$ and $\mathbf{k}_2$ near $\mathbf{k}_0$ arrive at the detector. They have the same group-velocity direction, but arrive at slightly different times because $|\mathbf{v}_1|\neq|\mathbf{v}_2|$. We assume that the pulse length is sufficiently long that the two pulses can interfere over most of their duration [9]. If we further assume that $\mathbf{k}_1$ and $\mathbf{k}_2$ are close to $\mathbf{k}_0$, and that $\mathbf{q}\equiv\mathbf{k}_1-\mathbf{k}_0\approx\mathbf{k}_0-\mathbf{k}_2$, then the two waves destructively interfere if their total phase difference through the sample, $2\mathbf{q}\cdot\mathbf{R}_1$, is an odd integer multiple of π.

Defining the Cartesian coordinate axes q_1,q_2,q_3 with the origin at $\mathbf{k}_0$, q_3 along $\mathbf{v}_0$, and q_1 in the plane, as shown in Fig. 2(a), the constant-ω curve near the parabolic

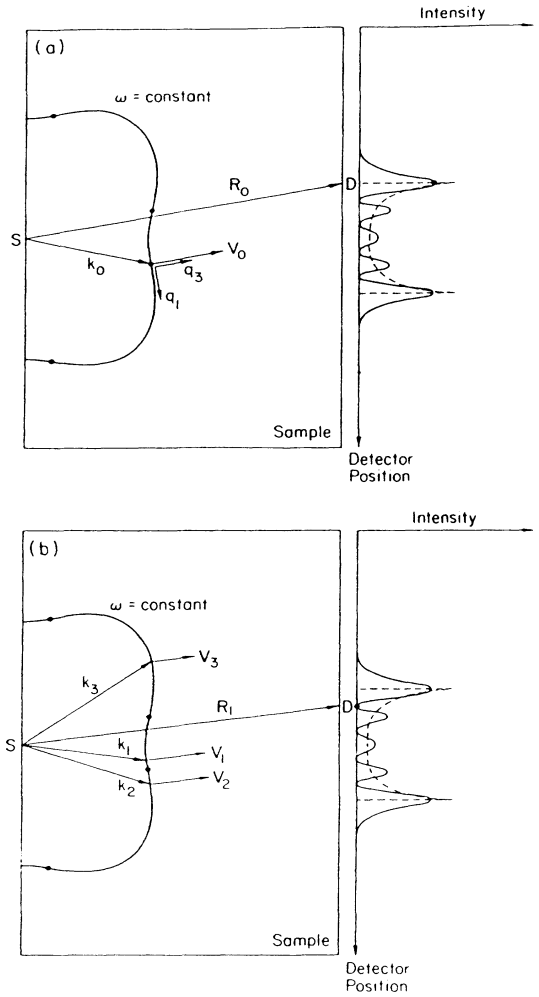

FIG. 2. Schematic of phonon focusing for ultrasound waves originating at S and detected at D. The constant-ω surface is for silicon. The plot on the right indicates the detected intensity. The dotted line is the intensity in the high-frequency limit; the solid line is for long-wavelength ultrasonic waves. (a) For $\mathbf{k}=\mathbf{k}_0$, the group velocity is $\mathbf{V}_0$ and the ray arrives at $\mathbf{R}_0$. (b) There are three $\mathbf{k}$'s with $\mathbf{V}$'s such that the rays arrive at $\mathbf{R}_1$. The phase velocities of these rays are different, so they have different phases at $\mathbf{R}_1$ and interfere.

point can be parametrized as $q_3=-aq_1^3/k_0^2$. Using a little geometry, one can show that

$$q_1\approx(\pi k_0^2/4aR_1)^{1/3} \quad (1)$$

gives destructive interference between $\mathbf{k}_1$ and $\mathbf{k}_2$. The fringes resulting from this effect are shown schematically in Fig. 2. Based on this estimate for $\mathbf{q}$, the angles of the real-space fringes scale as

$$\theta\propto(a/k_0^2R_1^2)^{1/3}. \quad (2)$$

Unlike the standard two-slit diffraction problem in which the fringe angles are independent of the source-to-detector distance R_1, the angles of the fringes here scale

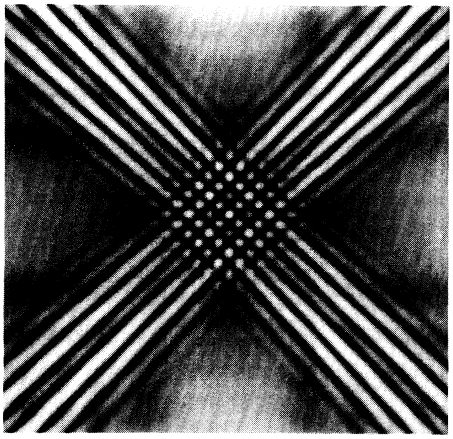

FIG. 3. Theoretical ultrasound image of a 2-cm cube of silicon at 15 MHz, covering the same scan range as Fig. 1(b) and based on the model of Eq. (3).

as $R_1^{-2/3}$, and on the wavelength as $\lambda_0^{2/3}$ rather than λ_0^1.

To fully understand the effects of finite wavelengths on the focusing patterns, we must deal with the full three-dimensional anisotropy of the crystal. In some directions this leads to many more than two interfering waves, all of which must be included in the analysis. We employ a model based on the superposition of plane waves, as used by Maris [5]. In this model, the displacement amplitude due to the elastic wave is given by

$$\mathbf{u}(\mathbf{R},\omega)=\int_\Omega d^2k\,\frac{\mathbf{f}(\omega,\mathbf{k})}{|\mathbf{V}(\mathbf{k})|}e^{i\mathbf{k}\cdot\mathbf{R}}, \tag{3}$$

where the integral in k space is over the constant-frequency surface $\Omega(\mathbf{k})=\omega$, and $\mathbf{V}$ is the group velocity. The factor $\mathbf{f}$ is calculated from an assumed incident stress distribution. The integral is then evaluated at points $\mathbf{R}$ on the detector surface.

For a 2-cm cube of silicon, evaluation of Eq. (3) at a frequency of 15 MHz and various $\mathbf{R}$ gives the image shown in Fig. 3, which agrees quite well with the experimental image of Fig. 1(b). In the long-wavelength limit the "thermal" caustics evolve into a set of parallel fringes as discussed above. The caustics forming the two box-shaped structures near the center of Fig. 1(a) are similarly replaced by an intense series of dots which appear in both the experimental and computed images. These qualitative features do not depend strongly on the assumed incident stresses, although relative intensities do.

We have also obtained ultrasonic patterns for metallic crystals and a polymer composite. The experimental image for aluminum is shown in Fig. 4(a). A calculated image for aluminum (not shown) is qualitatively similar to the data and indicates that the intense horizontal and vertical lines are associated with the ST mode. The radial modulations of these lines, however, are not reproduced by the theory. One possible explanation of this effect is

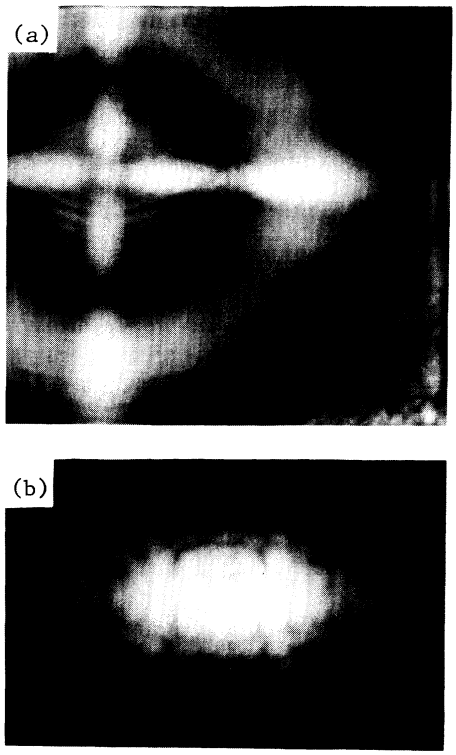

FIG. 4. (a) Experimental ultrasound image of single-crystal aluminum (200-ns pulse). The (100)-oriented sample is 7.3 mm thick, and the image covers a 12-mm-square region. (b) Experimental ultrasound image of a 1.8-mm-thick polymer composite (500-ns pulse).

pseudosurface waves [10]. Figure 4(b) is an image of a unidirectional laminated polymer composite, composed of eight nominally identical layers of fiber in epoxy. The anisotropy in wave intensity, as in the crystalline case, arises from the effective homogeneous elastic anisotropies of the material.

We have presented the first experimental evidence of the predicted finite-wavelength effects associated with phonon focusing. The demonstrated ability to characterize the propagation of ultrasound as a continuous function of direction, and to distinguish wave polarization by the characteristic intensity patterns of each acoustic mode, should permit the study of a wide range of phenomena in solids. We anticipate probing interactions between electrons and acoustic waves in metals, semiconductors, and superconductors, examining phase transitions in solids, and assessing the anisotropy of engineered composite materials.

We thank B. Cabrera for supplying the Si crystal, A. V. Granato for the Al crystal, and N. Sottos for the polymer composite. This work was supported by the National Science Foundation under Materials Research Laboratory Grant No. DMR-89-20538 and by the National Science Foundation's Solid Mechanics Program through Grant No. MSS-91-14360. M.R.H. is supported by an

IBM Predoctoral Fellowship.

[1] B. Taylor, H. J. Maris, and C. Elbaum, Phys. Rev. Lett. **23**, 416 (1969); Phys. Rev. B **3**, 1462 (1971).
[2] H. J. Maris, J. Acoust. Soc. Am. **50**, 812 (1971).
[3] For a review, see G. A. Northrop and J. P. Wolfe, in *Nonequilibrium Phonon Dynamics*, edited by W. E. Bron (Plenum, New York, 1985), Chap. 5.
[4] J. A. Shields and J. P. Wolfe, Z. Phys. B **25**, 11 (1989).
[5] H. J. Maris, Phys. Rev. B **28**, 7033 (1983).
[6] The feasibility of using ultrasonic waves to observe the focusing of phonons and finite-wavelength effects was suggested by V. V. Novikov and L. A. Chernozatonskii, Akust. Zh. **34**, 362 (1988) [Sov. Phys. Acoust. **34**, 215 (1988)].
[7] A. G. Every, W. Sachse, K. Y. Kim, and M. O. Thompson, Phys. Rev. Lett. **65**, 1446 (1990).
[8] A. G. Every and W. Sachse, Phys. Rev. B **42**, 8196 (1990).
[9] The existence of several distinct $\mathbf{k}$'s with the same $\mathbf{V}$ direction results in a folded group-velocity surface or "wave surface" [3]; the interfering waves originate from different sheets on this surface. There are actually three wave vectors with group velocities in the $\mathbf{R}_1$ direction in Fig. 2. $\mathbf{k}_3$ is not considered because its group velocity is much slower, hence such waves arrive too late to interfere with $\mathbf{k}_1$ and $\mathbf{k}_2$. A similar $\mathbf{k}$ with $\mathbf{V} \| \mathbf{V}_0$ is not shown in Fig. 2(a).
[10] A. G. Every, G. L. Koos, and J. P. Wolfe, Phys. Rev. B **29**, 2190 (1984).

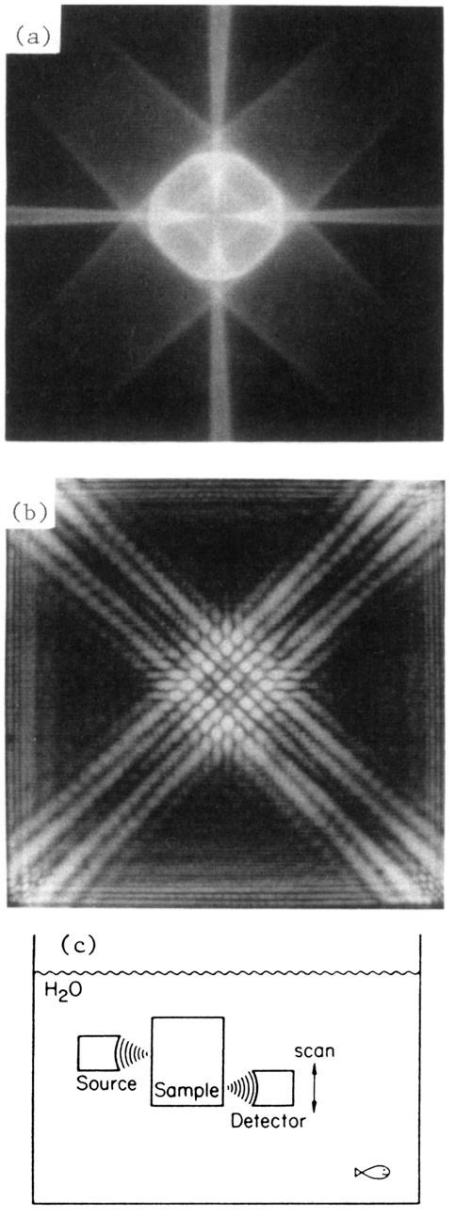

FIG. 1. (a) High-frequency phonon image of a (100)-oriented 2-cm silicon cube (1.5-cm×1.5-cm scan range). (b) 15-MHz ultrasound image of the same 2-cm silicon cube over the entire face (500-ns pulse). (c) Schematic of ultrasound experiment.

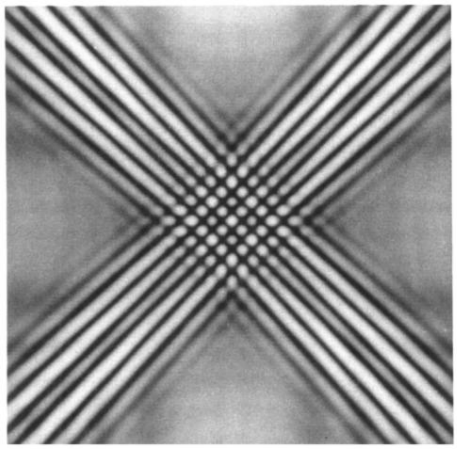

FIG. 3. Theoretical ultrasound image of a 2-cm cube of silicon at 15 MHz, covering the same scan range as Fig. 1(b) and based on the model of Eq. (3).

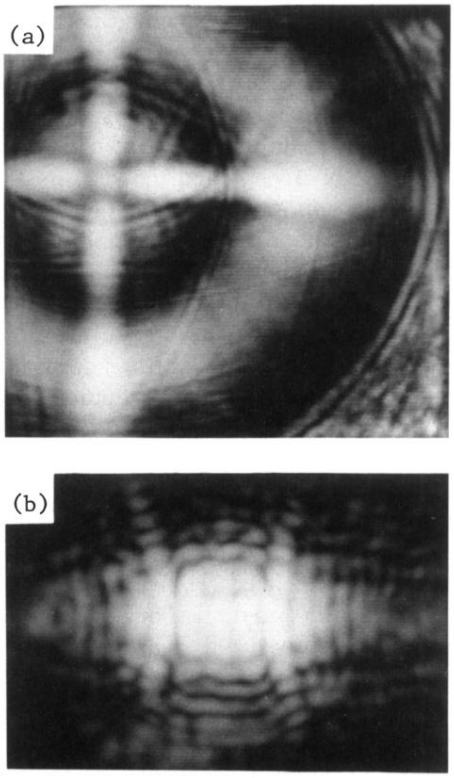

FIG. 4. (a) Experimental ultrasound image of single-crystal aluminum (200-ns pulse). The (100)-oriented sample is 7.3 mm thick, and the image covers a 12-mm-square region. (b) Experimental ultrasound image of a 1.8-mm-thick polymer composite (500-ns pulse).